

Spring 5-2-2011

Hydrodynamics of a Loop-seal Operated in a Circulating Fluidized Bed: Influence of The Operating Conditions on Gas and Solid Flow Patterns

Roberto Solimene

Istituto di Ricerche sulla Combustione – CNR, solimene@irc.cnr.it

Riccardo Chirone

CNR, Italy, chirone@irc.na.cnr.it

Piero Bareschino

Università degli Studi del Sannio, piero.bareschino@unisannio.it

Piero Salatino

Università degli Studi di Napoli Federico II, Italy, piero.salatino@unina.it

Follow this and additional works at: <http://dc.engconfintl.org/cfb10>

 Part of the [Chemical Engineering Commons](#)

Recommended Citation

Roberto Solimene, Riccardo Chirone, Piero Bareschino, and Piero Salatino, "Hydrodynamics of a Loop-seal Operated in a Circulating Fluidized Bed: Influence of The Operating Conditions on Gas and Solid Flow Patterns" in "10th International Conference on Circulating Fluidized Beds and Fluidization Technology - CFB-10", T. Knowlton, PSRI Eds, ECI Symposium Series, (2013).
<http://dc.engconfintl.org/cfb10/9>

This Conference Proceeding is brought to you for free and open access by the Refereed Proceedings at ECI Digital Archives. It has been accepted for inclusion in 10th International Conference on Circulating Fluidized Beds and Fluidization Technology - CFB-10 by an authorized administrator of ECI Digital Archives. For more information, please contact franco@bepress.com.

HYDRODYNAMICS OF A LOOP-SEAL OPERATED IN A CIRCULATING FLUIDIZED BED: INFLUENCE OF THE OPERATING CONDITIONS ON GAS AND SOLID FLOW PATTERNS

Roberto Solimene¹, Riccardo Chirone¹, Piero Bareschino³, Piero Salatino²

¹Istituto di Ricerche sulla Combustione – CNR

²Dipartimento di Ingegneria Chimica - Università degli studi di Napoli Federico II
Piazzale Tecchio, 80 80125 Napoli Italy

³Dipartimento di Ingegneria – Università degli Studi del Sannio
Piazza Roma, 21 82100 Benevento Italy

T: +390817682237; F: +390815936936; E: solimene@irc.cnr.it

ABSTRACT

Hydrodynamic features of a loop-seal operated as solids re-injection device in a lab-scale cold CFB apparatus are studied. Gas flow patterns are characterized by means of gas tracing experiments with continuous injection of CO₂ in the loop-seal chambers. Solids flow patterns are characterized by impulsive injection of dye-coloured particles into the supply chamber, followed by particle tracking.

INTRODUCTION

The dual fluidized bed technology has recently risen to renewed interest for process applications whenever distinct reactive environments (e.g. oxidative/reducing, temperature and/or pressure looping) need to be established while sharing a solid stream which acts as reactant or thermal carrier. Exploitation of the dual fluidized bed concept is currently being explored in fields like: i) CO₂ capture in coal-fired generating stations and cement kilns (1); ii) chemical-looping combustion (2-3); iii) biomass pyrolysis and gasification (4). The dual loop system presents, however, some criticalities that are mostly related to the effective control of solids recirculation between the beds and to the establishment of leak-tight operation of the beds with respect to the gaseous streams. These criticalities involve both design and operational variables of the plant which determine the hydrodynamic behaviour of different plant components (5-6). Several types of non-mechanical valves (L-valve, J-valve, seal pot and loop-seal) are commonly used in CFBs and DIFBs to control the mass flow rate of solids or to seal gaseous streams. Despite empirical or semi-empirical criteria for correct loop-seal design have been laid (7-15), thorough characterization of loop-seal hydrodynamics, especially under large solid throughput conditions, is still lacking. In the present study the hydrodynamics of a loop-seal is investigated. The seal is operated as solids re-injection device between a 40 mm ID downcomer and a 102 mm ID riser in a lab-scale cold CFB apparatus. The experimental procedure includes time-resolved measurements of gas pressure at several locations along the CFB loop and in the loop-seal and of solids mass flux along the riser. The gas flow patterns are characterized according to tracing methods based on continuous CO₂ injection at the bottom of the loop-seal chambers. Solids flow patterns are characterized by impulsive injection of dye-

coloured particles into the supply chamber, followed by particle tracking by means of a video camera interfaced to a computer. The characterization of the gas and solids flow patterns is carried out under a broad range of operating conditions by varying: i) the gas superficial velocity in the riser; ii) the fluidization velocity in the loop seal; iii) the throughput of circulating bed solids in the loop seal. Results are presented and discussed with an emphasis on the establishment of gas cross-flow between the loop seal chambers and its relevance to effective solids recirculation and gas “leakage”.

EXPERIMENTAL

Apparatus

The lab-scale cold model CFB (Figure 1) consisted of a riser, a cyclone, a solids reservoir, a standpipe and a loop seal. The Plexiglas riser, 0.102 m ID and 5.6 m high, was equipped with a gas distributor consisting of several stainless steel nets layered one on the other up to 2 mm thickness, characterized by low-pressure drop. An high-efficiency cyclone, 0.09 m and 0.32 m high, was installed at riser outlet. The solids return line consisted of the solids reservoir, 180 mm ID 0.40 m high, a 40 mm standpipe and a loop seal. The supply and recycle chambers of the loop seal have a square cross section (50mm side), height of 300 and 250 mm, respectively, and separate wind-boxes. The gap at the bottom of the two chambers is about 50 mm. The CFB loop was equipped with 21 pressure taps at different locations. The overall solids mass flux was determined by closing for a pre-set time a butterfly valve located along the standpipe and measuring the solids mass accumulated upstream the valve.

Diagnostics

High-precision piezo-resistive gas pressure transducers have been adopted to measure the gas pressure along the CFB loop. An on-line gas sampling carried out by means of a probe connected to a CO₂ gas analyzer (ABB advance optima Uras 14) was optimized to investigate the gas flow in the loop seal. All signals coming from the instruments were logged on a data acquisition unit consisting of a PC equipped with a data acquisition board. A high-speed, highly light-sensitive megapixel CMOS camera interfaced to a computer and controlled with an image processing software has been adopted for particle tracking in the loop seal chambers.

Materials and Operating Conditions

Table 1 reports the properties of quartz adopted for the tests. Fluidizing gas was technical air at room temperature. Gaseous CO₂ from cylinders and black glass (500 μm) beads were used as gas and solids tracer, respectively. Solids inventory was 3.5 kg. Gas superficial velocity in the riser $U_{g,r}$ ranged between 2.1 and 4.4 m/s. The minimum value of $U_{g,r}$ was always larger than the terminal velocity (U_t) of the granular solid. Air was injected at the bottom of the loop-seal so that gas superficial velocity in loop-seal chambers ($U_{g,ls}$) results to be 1, 1.5 and 2 times U_{mf} . Solids mass circulation fluxes in the riser G_s ranged

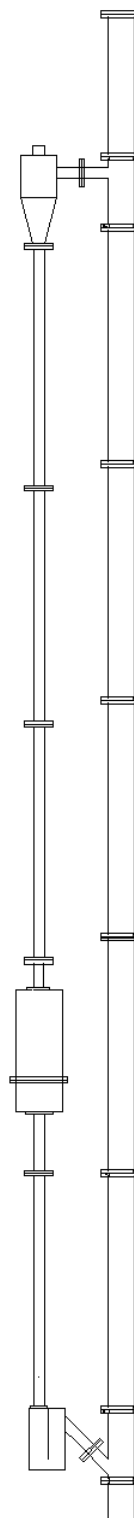


Fig. 1: Experimental apparatus.

between 2 and 11 kg/(s m²). Voidage (ε) along the riser was calculated by processing the pressure drops, ΔP , measured at successive pressure taps located at distance Δz according to the relationship $\Delta P = \rho_s g (1 - \varepsilon) \Delta z$, where g is the acceleration due to gravity.

Material	Quartz
Sauter mean diameter (d_p), μm	253
Size range, μm	100-400
Particle density (ρ_s), kg/m^3	2300
Incipient fluidization velocity (U_{mf}) ⁽¹⁾ , m/s	0.047
Terminal velocity (U_t) ⁽¹⁾ , m/s	1.77

⁽¹⁾ calculated

Procedure

Bed Hydrodynamics: Steady state operation of the CFB loop has been investigated at a pre-set fluidization velocity in the riser and in the loop seal. The steady state condition has been recognized by continuous monitoring of the gas pressure along the loop and by step-wise measurement of the mass flow rate. Once the steady state condition was reached, the gas pressure signal was acquired for about 5 minutes. The experiments have been characterized in terms of fluidization velocity both in the riser and in the loop seal.

Gas and Solids Tracing in the Loop Seal: Some experiments have been carried out to investigate the gas and solids flow patterns in the loop seal at $U_{g,r} = 2.85 \text{ m/s}$. Once the steady state operation of the CFB loop was reached at a pre-set $U_{g,ls}$, a batch of solids tracer (50g) was injected along the standpipe. The tracing particles fell down in the loop seal and their motion has been recorded by the video camera at 125 fps for 30s. The experiments has been repeated for three times and they have characterized in terms of $U_{g,ls}$. An ad-hoc procedure of image analysis has been developed to follow the trajectories of the tracing particles. In the same operating conditions, gas tracing has been carried out by continuous feeding of a gas fluidizing stream with a pre-set CO₂ concentration (in the range of 10-20%_v) in the supply and in the recycle chamber, alternatively. The CO₂ concentration has been measured at the bottom and the top of beds of the loop seal. The obtained data have been analyzed to achieve the gas flow distribution in the loop seal.

RESULTS AND DISCUSSION

Hydrodynamics of the Riser and of the Loop Seal: Figure 2 reports relative pressures measured at different pressure taps located around the CFB loop during runs operated at $U_{g,r} = 2.85 \text{ m/s}$. The gas superficial velocity in the loop seal $U_{g,ls}$ was varied in the range $U_{mf} \leq U_{g,ls} \leq 2U_{mf}$. Analysis of the pressure loop indicates that the pressure gradient at the bottom of the riser (i.e. at levels above the distributor up to 0.1m) increases as $U_{g,ls}$ is increased. The pressure gradient in the recycle chamber of the loop seal remains constant at a value consistent with the bulk density of the bed material under bubbling fluidization conditions at any $U_{g,ls}$. The pressure gradient in the supply chamber increases from a minimum at $U_{g,ls} = U_{mf}$ to approach values corresponding to the bulk density of a fully fluidized bubbling bed as $U_{g,ls}$ is increased. Figure 3 reports the solids mass flux in the riser as well as the pressure drop and the height of the bed of solids, respectively, in the recycle and in the supply chamber of the loop-seal. Data points correspond to the three experimental conditions reported in Figure 2. As $U_{g,ls}$ is increased the following features can be recognized: i) the solid mass flux remains substantially constant; ii) the pressure drop in the recycle chamber slightly decreases; ii) the pressure drop in the supply chamber undergoes a pronounced increase whereas the bed height decreases as

$U_{g,ls}$ increases from U_{mf} to $1.5U_{mf}$, both remaining nearly constant at values larger than U_{mf} . Altogether, the fluidization velocity in the loop seal exerts a moderate influence on riser hydrodynamics, whereas loop seal hydrodynamics is affected to a larger extent. As $U_{g,ls}$ was increased from U_{mf} to $1.5U_{mf}$, the bed material present in the supply chamber becomes fully fluidized, consistently with the change of pressure drop and gradient reported in Figures 2 and 3.

When the supply chamber is fluidized, a fraction of the solids present in this chamber is transferred to the riser, and the loading of solids at the bottom of the

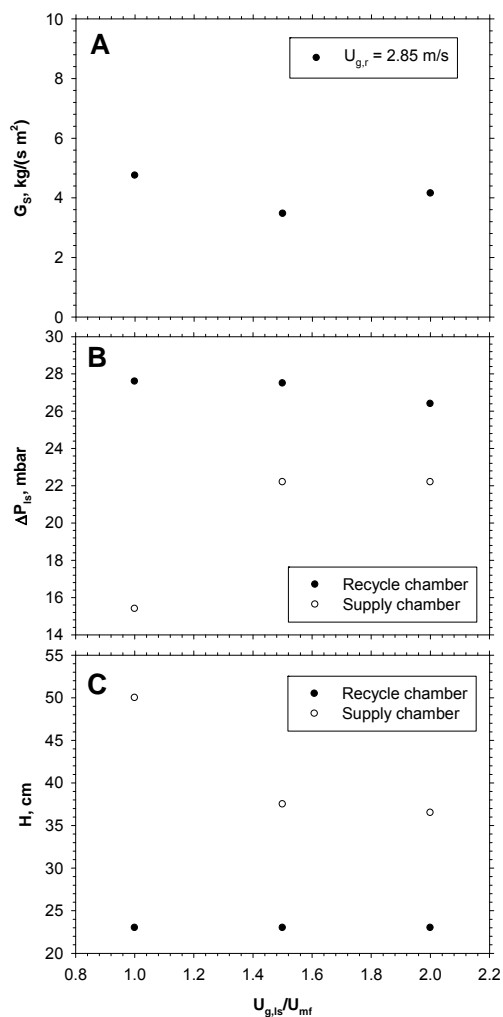


Fig. 3: Solids mass flux (A) pressure drops (B) and bed height (C) in the loop-seal chambers as a function of $U_{g,ls}/U_{mf}$ ratio. $U_{g,r}=2.85$ m/s.

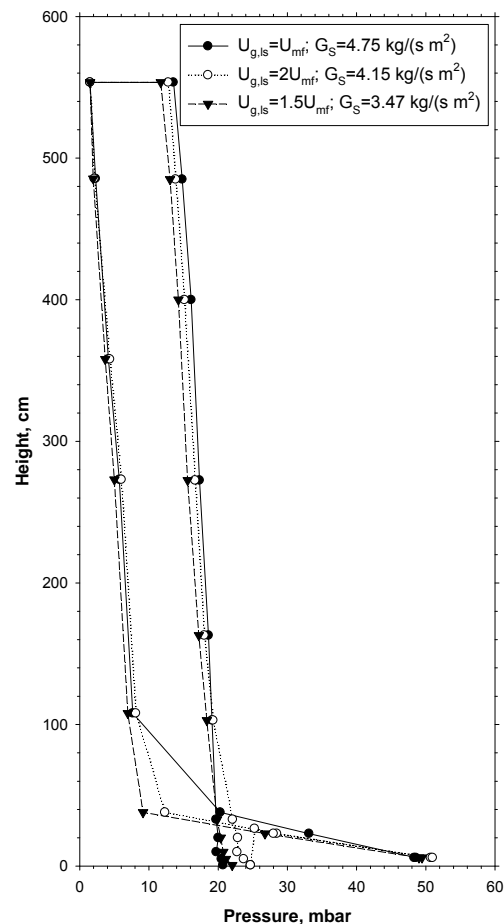


Fig. 2: Pressure loop for different $U_{g,ls}/U_{mf}$ ratio; $U_{g,r}=2.85$ m/s.

riser is increased. This feature is reflected by the change of bed height in the supply chamber and of the pressure gradient at the bottom of the riser. Figure 4 reports the solids mass flux in the riser and the bulk density (ρ) of the bed at the bottom of the riser as a function of the fluidization velocity ($U_{g,r}$) for different values of the ratio $U_{g,ls}/U_{mf}$ in the loop seal. The following features can be recognized: i) G_s increases almost linearly with $U_{g,r}$; ii) G_s is barely influenced by $U_{g,ls}/U_{mf}$, except for $U_{g,ls}=U_{mf}$ and for high values of $U_{g,r}$; iii) ρ is also barely influenced by $U_{g,ls}/U_{mf}$ except for $U_{g,ls}=U_{mf}$, when the values of ρ recorded are smaller regardless of $U_{g,r}$; iv) ρ remains substantially constant at a value of about 140kg/m^3 for $U_{g,r}>3\text{m/s}$, it increases as the fluidization velocity in the riser is decreased at $U_{g,r}<3\text{m/s}$; v) for values

of $U_{g,r} < 3\text{m/s}$, as the terminal velocity of bed particles is approached, a dense bed is established at the bottom of the riser with values of ρ in the order of $800\text{-}1000\text{kg/m}^3$. It can be concluded that loop seal operation in the CFB loop becomes fully effective when the supply chamber, and not only the recycle chamber, becomes fully fluidized. This condition requires the gas superficial velocity in the loop seal to exceed U_{mf} .

Analysis of Solids Flow Patterns in the Loop Seal:

Loop seal hydrodynamics has been also investigated by inspection of the gas and solids flow patterns in the loop seal chambers as $U_{g,ls}$ has been changed. Figure 5 shows the trajectory and the time-resolved components (V_x , V_y) of the instantaneous velocity of three tracer particles. Trajectories were reconstructed by frame-by-frame analysis of videorecordings taken during system operation at $U_{g,ls}$ equal to U_{mf} and $1.5U_{mf}$, with a riser gas superficial velocity set at $U_{g,r} = 2.85\text{m/s}$. Images acquired for $U_{g,ls} = 2U_{mf}$ could not be analyzed as the stochastic motion of the particles typical of a bubbling fluidized bed prevented to follow a single particle along the test. Trajectories are mapped in Figure 5 assuming as origin of the reference axes the bottom-left corner of the supply chamber, taking x positive along the direction pointing toward the riser and y positive along the direction opposed to gravity. The tracer particles were selected as they were at the top of the supply chamber: one at the center and the other two near the external wall and the separation wall (vertical solid line) with the recycle chamber, respectively. The tracer particles were then followed frame by frame during their motion toward and beyond the gap between the loop seal chambers. At $U_{g,ls} = U_{mf}$, the following features can be recognized: i) the streamlines followed by the tracer particles in the supply chamber converge toward the top of the gap between the chambers; ii) a significant part of the supply chamber bottom appears stagnant (below the dashed line); iii) a limited part of the gap between the two loop seal chambers is characterized by flow of bed solids; iv) the velocity component along the x axis (V_x) is substantially similar for all the tracer particles and constant with time (about 1.5mm/s), but it increases significantly as they approach the gap between the two chambers; v) the velocity component along the y axis (V_y) is similar for all the tracer particles and decreases as they approach the gap between the two chambers; vi) the tracer particle initially close to the supply chamber axis presents the largest value of V_y ; vii) V_y is negative and positive in the supply and recycle chamber, respectively. Increasing $U_{g,ls}$ ($U_{g,ls} = 1.5U_{mf}$), it can be recognized that: i) convergence of the trajectories followed by the tracer particles in the supply chamber takes place at a later stage close to the

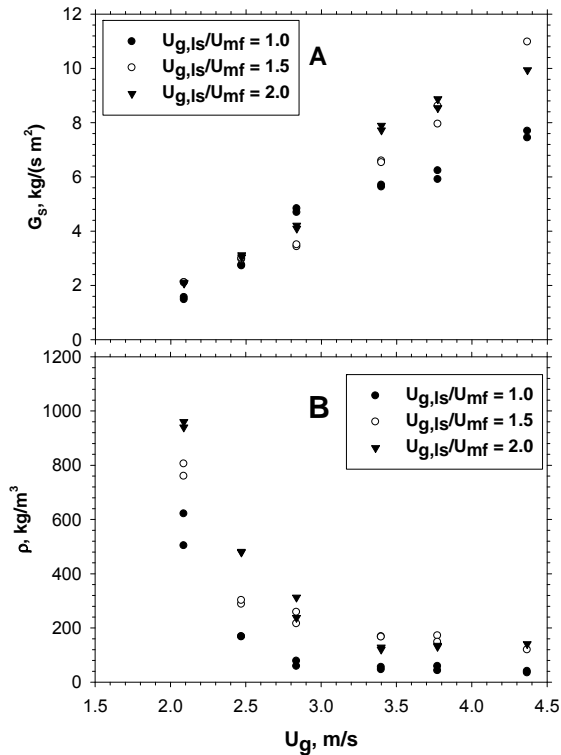


Fig. 4: Solids mass flux (A) and bottom bulk density (B) as a function of $U_{g,r}$ for different $U_{g,ls}/U_{mf}$ ratio.

upper part of the gap between the two chambers; ii) the stagnant region at supply chamber bottom is less extended than that observed at $U_{g,ls}=U_{mf}$; iii) the fractional area of the gap between the two chambers where solids flow takes place to a significant extent, is expanded; iv) V_x is initially negligible for all the tracing particles except when they approach the gap; v) V_y is similar for all the tracer particles and constant with time (about 12.5 mm/s) in the supply chamber; it becomes positive and increases with time in the recycle chamber; vi) the tracer particle initially located close to the external wall impinges the stagnant region and stops there. In the range $U_{mf} < U_{g,ls} < 1.5U_{mf}$ the bed solids motion in the supply chamber can be accurately described by streamlines being the random effect due to bubble motion negligible, whereas at $U_{g,ls}=2U_{mf}$, the stagnant region disappears and bubbling fluidization conditions established throughout the bed.

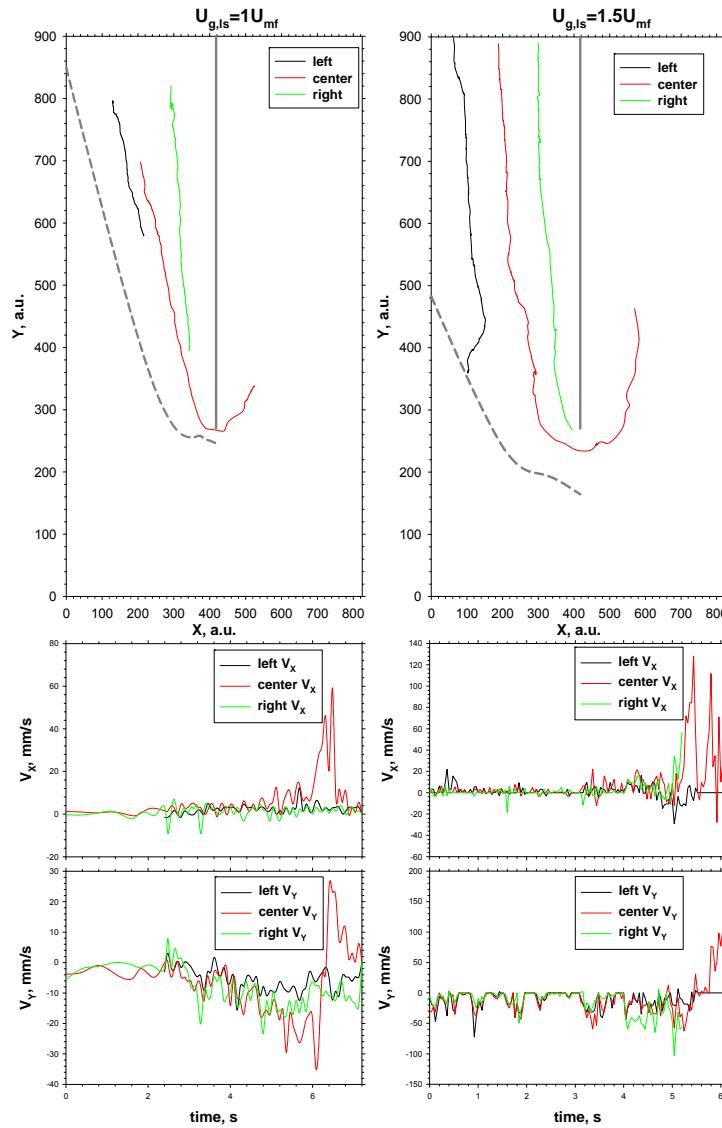


Fig. 5: Loop seal solids flow patterns: trajectory and time-resolved instantaneous velocity of three tracing particles as a function of $U_{g,ls}$.

Analysis of gas flow patterns in the loop seal from gas tracing experiments:

Figure 6 shows a schematic sketch of the gas flow pattern in the loop seal during gas tracing experiments. Two separate gas streams of equal flow rates are fed to the bottom of the supply (Q_{SC}^{in}) and recycle (Q_{RC}^{in}) chambers of the loop seal, characterized by different CO_2 concentrations x_{SC}^{in} and x_{RC}^{in} , respectively. Experiments have been carried out at a pre-set inlet concentration both in the supply and recycle chamber and in the same operating conditions of bed solids tracing ($U_{g,r}=2.85\text{m/s}$, $U_{g,ls}=U_{mf}$, $1.5U_{mf}$, $2U_{mf}$). The gas cross-flow between the two chambers has been represented by two streams: one (Q_{RC}^{bypass}) directed from the recycle chamber toward the supply chamber, the other (Q_{SC}^{bypass}) in the opposite direction. It has been assumed that the by-pass stream CO_2 concentration is that of the inlet gas flow rate at the corresponding chamber. From the known values of

Q_{SC}^{in} , Q_{RC}^{in} , x_{SC}^{in} , x_{RC}^{in} and the measured values of the CO₂ concentration (x_{SC}^{out} , x_{RC}^{out}) at the outlet, it is possible to calculate all the other gas flow rates (Q_{RC}^{bypass} , Q_{SC}^{bypass} , Q_{SC}^{out} and Q_{RC}^{out}) on the basis of global material balance and on a balance on CO₂. Figure 7 shows x_{SC}^{in} , x_{RC}^{in} , x_{SC}^{out} and x_{RC}^{out} as a function of $U_{g,ls}$ during gas tracing experiments in both loop seal chambers. It can be recognized that: i) x_{SC}^{out} is nearby to x_{SC}^{in} both when a pre-set CO₂ concentration is fed to the supply chamber (supply chamber gas tracing) and when only air is used as fluidizing gas (recycle chamber gas tracing); ii) x_{RC}^{out} shows departures from x_{RC}^{in} : it is smaller than the inlet pre-set CO₂ concentration when gas tracing occurs in the recycle chamber and it is larger than air CO₂ concentration when gas tracer is fed to the supply chamber. On the basis of the data reported and on the material balances, the calculated Q_{RC}^{bypass} is negligible (in order of 0.01m³/h), whereas Q_{SC}^{bypass} does not significantly depend on $U_{g,ls}$ and it is about 0.2m³/h. Taking into account that the minimum fluidization gas flow rate is about 0.45m³/h for a single chamber, Q_{SC}^{bypass} represents a significant fraction of the effective gas superficial velocity in the supply chamber. The fluidization condition in the supply chamber can be approximately based on the following simplified relationship:

$$U_{g,ls}^{eff} \geq U_{mf} - \frac{G_s A_r \epsilon_{mf}}{A_{ls} \rho_s (1 - \epsilon_{mf})} \quad (1)$$

where $U_{g,ls}^{eff}$, ρ_s , ϵ_{mf} , A_r , A_{ls} are the effective gas superficial velocity, bed solids density, bed voidage at incipient fluidization, cross sections of the riser and of the supply chambers, respectively. Equation (1) expresses the net gas superficial velocity established in the emulsion phase of the bed in the supply chamber when the downflow of bed solids is taken into account. This value could be negative for low values of U_{mf} or large values of G_s . It is worth noting that a negative value of $U_{g,ls}^{eff}$ is not *per se* undesirable from the standpoint of an effective recirculation of solids, but it is extremely important when "leakage" of gas from the supply chamber

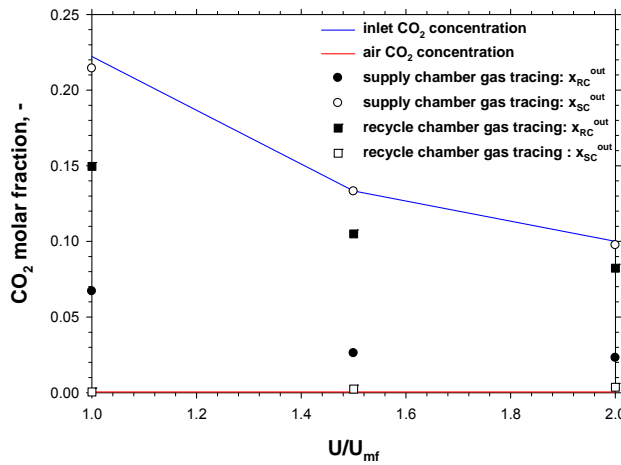


Fig. 7: Inlet and outlet CO₂ concentrations in the loop seal chambers as a function of $U_{g,ls}$ during gas tracing experiments.

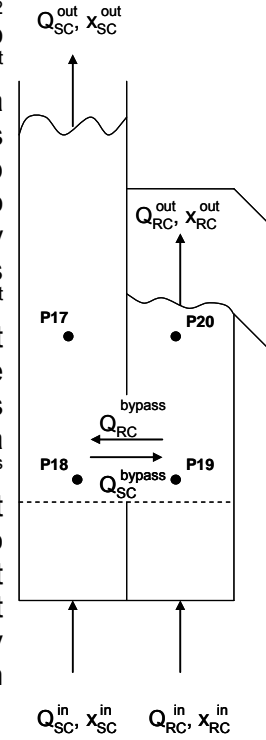


Fig. 6: Schematic sketch of the gas flow pattern in the loop seal.

to the recycle chamber must be required by process constraint. This is the case, for instance, when the loop seal is part of a dual interconnected fluidized bed-system with distinct reactive environments. The relationship (1) is satisfied in all the experimental conditions tested, except for those carried out at $U_{g,ls} = U_{mf}$. Under this condition, the supply chamber of the loop seal is largely unfluidized, consistently with the pressure drop data and with the analysis of bed solids tracing.

CONCLUSIONS

The hydrodynamics of a loop-seal operated as solids re-injection device in a lab-scale cold CFB apparatus was characterized by a combination of methods, including solids and gas tracing. For a given riser gas superficial velocity, the loop seal fluidization velocity exerts a limited influence on riser hydrodynamics, but significantly modifies the gas and solids flow patterns in the loop-seal. As the loop seal is kept at gas superficial velocities just beyond incipient fluidization, the supply chamber is only partly fluidized and an extended stagnant zone is observed at its bottom. As fluidization becomes more vigorous, stagnant zone extension is reduced and more solids are transferred to the riser. Analysis of solids and gas tracing tests highlights the role of solids downflow in the supply chamber and of gas cross-flow from the supply to the recycle chamber on the fluidization patterns. An approximate criterion is given for the onset of gas "leakage" between the two loop seal sections, relevant to loop seal applications in dual interconnected fluidized beds.

NOTATION

A_{lp}	loop seal cross section [m ²]	V_x	horizontal velocity of tracing particle [m/s]
A_r	riser cross section [m ²]	V_y	vertical velocity of tracing particle [m/s]
d_p	particle size [μ m]	x_{RC}^{in}	recycle chamber inlet CO ₂ molar fraction [gmol/gmol]
g	acceleration due to gravity [m/s ²]	x_{RC}^{out}	recycle chamber outlet CO ₂ molar fraction [gmol/gmol]
G_s	solids mass flux [kg/m ² s]	x_{SC}^{in}	supply chamber inlet CO ₂ molar fraction [gmol/gmol]
P	gas pressure [Pa]	x_{SC}^{out}	supply chamber outlet CO ₂ molar fraction [gmol/gmol]
Q_{RC}^{bypass}	recycle chamber by-pass flow rate [m ³ /s]	X	horizontal coordinate of tracing particle [a.u.]
Q_{RC}^{in}	recycle chamber inlet flow rate [m ³ /s]	Y	vertical coordinate of tracing particle, [a.u.]
Q_{RC}^{out}	recycle chamber outlet flow rate [m ³ /s]	z	riser axial coordinate [m]
Q_{SC}^{bypass}	supply chamber by-pass flow rate [m ³ /s]	ϵ	gas voidage [-]
Q_{SC}^{in}	supply chamber inlet flow rate [m ³ /s]	ϵ_{mf}	minimum fluidization gas voidage [-]
Q_{SC}^{out}	supply chamber outlet flow rate [m ³ /s]	ρ	bulk density at riser bottom [kg/m ³]
$U_{g,ls}$	loop seal gas superficial velocity [m/s]	ρ_s	particle density [kg/m ³]
$U_{g,ls}^{eff}$	effective loop seal gas superficial velocity [m/s]		
$U_{g,r}$	riser gas superficial velocity [m/s]		
U_{mf}	minimum fluidization velocity [m/s]		
U_t	particle terminal velocity [m/s]		

REFERENCES

1. Hughes, R. W., Lu, D. Y., Anthony, E. J., Macchi, A. (2005) Fuel Process. Technol., 86, 1523.
2. Kronberger, B., Lyngfelt, A., Löffler, G., Hofbauer, H. (2005) Ind. Eng. Chem. Res., 44, 546.
3. Hossain, M. M., de Lasa, H. I. (2008). Chem. Eng. Sci., 63, 4433.
4. Pfeifer, C., Proll, T., Punchner, B., Hofbauer, H. (2007) Fluidisation XII (Bi, X., Berruti, F., Pugsley, T., (Eds.)), Engineering Foundation New York, pp. 889.
5. Kaiser, S., Löffler, G., Bosch, K., Hofbauer, H. (2003). Chem. Eng. Sci., 58, 4215.
6. Bai, D., Issangya, A. S., Zhu, J.-X., Grace, J. R. (1997) Ind. Eng. Chem. Res., 36, 3898.
7. Cheng, L., Basu, P., Cen, K. (1998). Trans. Inst. Chem. Eng., 76, 761.
8. Cheng, L., Basu, P., (2000). Powder Tech., 103, 203.
9. Basu, P., Cheng, L., (2000). Trans. Inst. Chem. Eng., 78, 991.
10. Botsio, E., Basu, P. (2005) Can. J. Chem. Eng., 83, 554.
11. Kim, S. W., Namkung, W., Kim, S. D. (1999). Korean J. Chem. Eng., 16(1), 82.
12. Kim, S. W., Namkung, W., Kim, S. D. (1999). Chem. Eng. Technol., 24, 843.
13. Kim, S. W., Kim, S. D., Lee, D. H. (2002). Ind. Eng. Chem. Res., 41, 4949.
14. Kim, S. W., Kim, S. D. (2002). Powder Tech., 124, 76.
15. Basu, P., Buttler, J. (2009). Applied Energy, 86, 1723.